Correlated Electronic Structure of $La_3Ni_2O_7$ under Pressure

Viktor Christiansson,[1] Francesco Petocchi,[2] and Philipp Werner[1]
[1]Department of Physics, University of Fribourg, 1700 Fribourg, Switzerland
[2]Department of Quantum Matter Physics, University of Geneva, 1211 Geneva 4, Switzerland

(Received 14 June 2023; revised 25 August 2023; accepted 27 September 2023; published 15 November 2023)

Recently, superconductivity with a T_c up to 78 K has been reported in bulk samples of the bilayer nickelate $La_3Ni_2O_7$ at pressures above 14 GPa. Important theoretical tasks are the formulation of relevant low-energy models and the clarification of the normal state properties. Here, we study the correlated electronic structure of the high-pressure phase in a four-orbital low-energy subspace using different many-body approaches: GW, dynamical mean field theory (DMFT), extended DMFT (EDMFT) and GW + EDMFT, with realistic frequency-dependent interaction parameters. The nonlocal correlation and screening effects captured by GW + EDMFT result in an instability toward the formation of charge stripes, with the $3d_{z^2}$ as the main active orbital. We also comment on the potential relevance of the rare-earth self-doping pocket, since hole doping suppresses the ordering tendency.

DOI: 10.1103/PhysRevLett.131.206501

Introduction.—Nickelates have been theoretically proposed more than 20 years ago as an interesting material platform to search for high-T_c superconductivity [1], but they have moved into the spotlight of the condensed matter community only after the recent experimental discovery of superconductivity in thin films of $Nd_{1-x}Sr_xNiO_2$ and $Pr_{1-x}Sr_xNiO_2$ with $x \approx 0.2$ [2–4]. Apart from these hole-doped infinite-layered systems, superconductivity has also been demonstrated in the quintuple layer compound $Nd_6Ni_5O_{12}$ [5], which realizes a favorable Ni-d filling for superconductivity, even without chemical doping [6]. The highest T_c values measured in these compounds so far are, however, substantially lower than in cuprates (maximum T_c of 31 K realized under pressure [7]), and superconductivity has not been observed in bulk crystals. The reported bulk superconductivity with a T_c near 80 K in the bilayered perovskite nickelate $La_3Ni_2O_7$ under pressure by Sun *et al.* [8], and shortly afterward by Zhang and coworkers [9], thus appears to be a major breakthrough, which will stimulate the research on high-temperature superconductivity [10–12].

An important theoretical challenge is the formulation of a minimal model which captures the relevant low-energy physics. In the case of cuprates, many researchers believe that a single-band Hubbard model, effectively representing the physics of the $d_{x^2-y^2}$ and oxygen states, provides an adequate starting point [13]. Indeed, qualitatively correct phase diagrams have been obtained with many-body treatments of this model [14]. In the case of the infinite-layer nickelates, the situation is less clear. It has been pointed out early on that due to the larger energy separation between the d and p bands, the low-energy physics of the nickelates differs from that of hole-doped charge-transfer insulators like the cuprates [15]. The important role of multiorbital effects, involving especially the d_{z^2} orbital in hole-doped nickelates, has also been emphasized [16,17]. On the other hand, based on the close similarity between the experimental T_c dome and the results from single-band calculations, it has been argued that the $d_{x^2-y^2}$ orbital plays the dominant role in nickelates, and that the single-band Hubbard model represents an adequate starting point [18].

Density functional theory (DFT) calculations for the high-pressure $Fmmm$ phase of the $La_3Ni_2O_7$ bilayer system suggest a low-energy model involving two $d_{x^2-y^2}$ and two d_{z^2} Ni orbitals [8], where the latter form bonding and antibonding states due to the strong interlayer hopping through the apical oxygen. A total of three electrons occupy the $d_{x^2-y^2}$ and the bonding states, which at the DFT level results in three partially filled metallic bands. An important question is how this picture is modified if the electronic correlations are treated with advanced many-body techniques. Here, we calculate the dynamically screened interaction parameters for the four-orbital low-energy model from first principles [19], and use them to compute the electronic structure with the GW approximation [20], dynamical mean field theory (DMFT) [21], extended DMFT (EDMFT) [22], and GW + EDMFT [23–25].

DFT calculation and cRPA interactions.—We start from a DFT calculation [26,27] of the high-pressure $Fmmm$ phase of bilayer $La_3Ni_2O_7$, which contains a single formula unit in the primitive cell with one Ni atom in each of the two layers. We perform calculations for the experimentally reported lattice parameters [8], at the three pressures $P = 20.9$, 29.5, and 41.2 GPa, covering the range where superconductivity has been observed. The atomic positions are fully relaxed. Compared to its infinite-layered counterparts, the rare-earth self-doping pocket at the Γ point in the

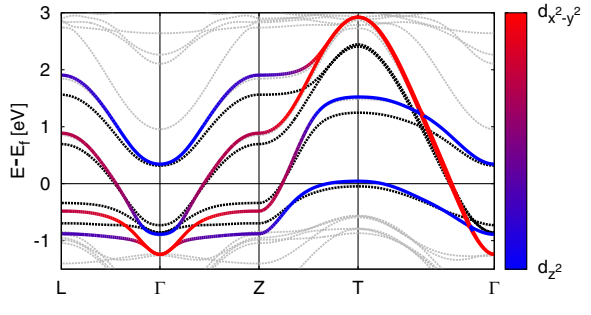

FIG. 1. The model band structure (solid lines) plotted on top of the DFT band structure (gray dashed lines). The color bar shows the orbital character of the model bands. We also indicate the G^0W^0 quasiparticle band structure by the black dashed line, showing a narrowing of the model bands and the disappearance of the hole pocket at the T momentum.

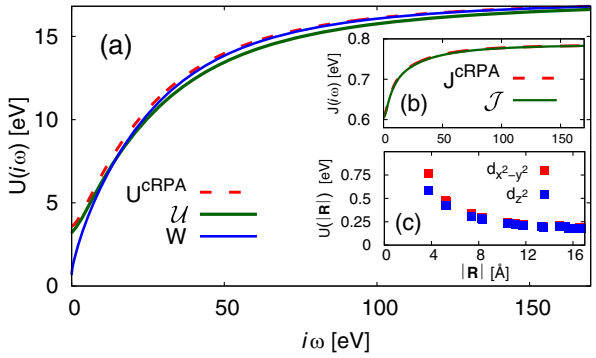

FIG. 2. (a) Frequency dependence of the bare local interactions for the d_{z^2}-like orbital, calculated within cRPA (U) and $GW+$ EDMFT ($\mathcal{U}$), as well as the fully screened interaction W. The insets show (b) the cRPA J and the $GW+\mathrm{EDMFT}$ effective Hund's couplings $\mathcal{J}$. (c) The nonlocal interaction $U(|\mathbf{R}|)$ within a single layer at different lattice spacings in Å for the $d_{x^2-y^2}$- and d_{z^2}-like orbitals.

DFT band structure is lifted above the Fermi level. It is important to note, however, that if we fix the atomic positions at the experimentally reported values [8], this band is lowered by 1 eV, leading again to a self-doping situation, see Supplemental Material (SM) [28]. We will comment on the potential relevance of this pocket in the discussion of the $GW+\mathrm{EDMFT}$ results.

Using the relaxed structure, we define a four orbital low-energy model of $d_{x^2-y^2}$- and d_{z^2}-like Wannier functions [32,33] on the two Ni sites. In Fig. 1 we show the resulting Wannier band structure (solid lines) overlayed on the DFT one (gray dashed lines). The full band structure is then downfolded to this low-energy subspace using the multitier approach of Refs. [24,25], with a constrained random-phase approximation (cRPA) [19] calculation to obtain the momentum- and frequency-dependent effective bare interaction parameters, and in the case of the GW-based methods a one-shot G_0W_0 calculation [20] to compute the effective bare propagators $G^0_{\mathbf{k}}(\omega)$ of the model. In the (E)DMFT calculations, unless otherwise noted, we solve separate impurity problems for each lattice site (see SM [28] and Refs. [39,40] for additional details). In the case of GW and $GW+\mathrm{EDMFT}$ the approach is free from double countings and adjustable parameters (apart from the choice of the low-energy subspace), while in DMFT and EDMFT we use the fully localized limit double counting prescription [41–43].

The effective interaction parameters of a low-energy model typically exhibit a large frequency dependence, especially for the density-density terms, while the Hund coupling parameter J is less screened. In Fig. 2 we show the cRPA result for the local ($\mathbf{R}=0$) components of the d_{z^2}-like orbital, and compare it to the self-consistently calculated effective bare interaction $\mathcal{U}$ and fully screened interaction W from the $GW+\mathrm{EDMFT}$ calculations. The static ($\omega=0$) values of the local interactions are

$$U_{\mathrm{cRPA}}=\begin{pmatrix} d_{x^2-y^2} & d_{z^2} \\ 3.79 & 2.39 \\ 0.61 & 3.58 \end{pmatrix}, \quad \mathcal{U}=\begin{pmatrix} d_{x^2-y^2} & d_{z^2} \\ 3.46 & 2.04 \\ 0.61 & 3.18 \end{pmatrix},$$

where the upper triangular part lists the density-density interactions and the lower left entry the Hund's coupling. Since $\mathcal{U}$ takes into account nonlocal screening within the model subspace, the density-density terms are reduced compared to cRPA. The nonlocal components of the cRPA interaction are comparatively large, with an in-plane nearest-neighbor interaction of ∼0.75 eV for the $d_{x^2-y^2}$-like orbital, indicating a need for considering nonlocal screening effects. The long-ranged ($\sim(1/r)$) tail of the bare interactions is demonstrated in Fig. 2(c) for translations within the bilayer.

The static interaction parameters remain almost unaffected by hydrostatic pressure, with changes of less than 0.05 eV, in contrast to the infinite-layered system where we found nontrivial systematic changes as a function of (uniaxial) pressure [40]. More detailed information on the local and nonlocal interactions and their pressure dependence is provided in the SM [28].

GW results.—As a first test of the (nonlocal) screening and correlation effects, we perform self-consistent GW calculations for our model, taking into account the full band structure through the downfolded interactions and propagators. The quasiparticle band structure corresponding to the initial $G^0_{\mathbf{k}}(\omega)$ is shown by the black dashed lines in Fig. 1. The main effect of self-consistency is a slight renormalization of the bands and a transfer of charge between the Ni orbitals, bringing them closer to quarter and half-filling, respectively, as indicated in Table I. Overall, the physical picture remains similar to DFT, with a filled bonding band of d_{z^2} character and two approximately quarter-filled bands of $d_{x^2-y^2}$ character [8]. The fact

TABLE I. Orbital occupation per spin n^i at inverse temperature $\beta = 50$ eV^{-1} (~230 K) and pressure $P = 29.5$ GPa for the Ni$_i$ $3d_{x^2-y^2}$- and $3d_{z^2}$-like orbitals in the two layers i of the primitive unit cell. The total filling is $n = 3$. GW + EDMFT results are shown for calculations with ordering (period-2 oscillations) and for suppressed order (SO), as discussed in the text. The calculations for the supercell, performed at $\beta = 10$ eV^{-1}, also result in period-2 oscillations. In this case we show the average occupations for one of the Ni dimers.

Method	$n^1_{x^2-y^2}$	$n^1_{z^2}$	$n^2_{x^2-y^2}$	$n^2_{z^2}$
DFT	0.31	0.44	0.31	0.44
scGW	0.23	0.52	0.23	0.52
DFT+DMFT $U^{\mathrm{cRPA}}(0)$	0.32	0.43	0.32	0.43
DFT+DMFT $U^{\mathrm{cRPA}}(\omega)$	0.37	0.38	0.37	0.38
EDMFT	0.50	0.51	0.32	0.17
GW + EDMFT	0.96	0.47	0.04	0.03
Supercell GW + EDMFT	0.90	0.53	0.04	0.03
GW + EDMFT (SO)	0.08	0.67	0.08	0.67

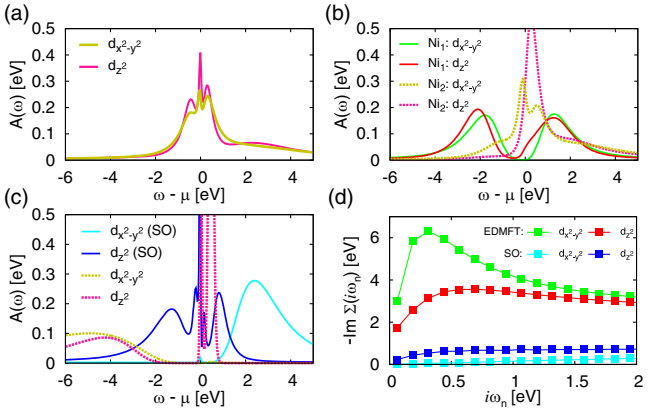

FIG. 3. Local spectral functions $A(\omega)$ for (a) DMFT+$U(\omega)$, (b) EDMFT, and (c) GW + EDMFT for the period-2 solution, and the solution with suppressed order (SO). (d) Imaginary part of the EDMFT self-energy [corresponding to the spectra in (b)] and GW + EDMFT result for suppressed order [corresponding to the spectra in (c)].

that the low-energy model has a bandwidth of ~4 eV, comparable to the on-site interactions, however, suggests that an accurate treatment of correlation effects requires calculations beyond DFT or GW.

DMFT and EDMFT results.—DMFT and EDMFT calculations provide a better description of local correlations by calculating a local self-energy (and local polarization function in the case of EDMFT) through a mapping of the lattice system to self-consistently determined impurity models [21,22,43]. We treat two separate impurity problems for the Ni sites in the two layers and do not use any mixing in the self-consistency loop, in order to detect potential ordering instabilities [44]. Our calculations down to inverse temperature $\beta = 50$ eV^{-1} (~230 K) show that for the static cRPA interactions, the orbital occupations within DFT + DMFT are very similar to the DFT results and previously reported DFT + U results [8], and that there is no ordering instability. We have checked that varying the static U values in a physically reasonable range between 3 and 5 eV does not change this picture (see SM [28]). In Table I we report the occupations obtained with both the static and frequency dependent local cRPA interactions. Taking into account the frequency dependence of the cRPA interactions leads to a transfer of charge to the $d_{x^2-y^2}$ orbital, resulting in a roughly equal filling in both orbitals. The latter result is qualitatively similar to recent DMFT calculations in Ref. [12], which, however, produced half-filled e_g orbitals. We believe that the discrepancy is due to the larger model subspace and different interactions parameters used in Ref. [12], which should also explain why our local DMFT spectra, shown in Fig. 3(a), are more metallic.

In the EDMFT calculations we take into account the local and nonlocal frequency dependent cRPA interactions, and treat dynamical screening effects in the low-energy subspace in the form of a local polarization. The nonlocal interactions lead to qualitative changes in the physics, compared to the previous methods. In particular, we now observe a breaking of the symmetry between the two Ni sites in the unit cell, corresponding to an emptying of one layer, and resulting in close to half-filled orbitals in the other layer. (Such a charge reshuffling between layers would likely result in a lattice response, which is not captured in our model.) The almost half-filled layer exhibits long-ranged antiferromagnetic (AFM) magnetic order, as indicated by oscillations between solutions with opposite spin polarizations in the self-consistency loop. The local spectral functions and self-energies shown in Figs. 3(b) and 3(d) reveal that the half-filled layer is nearly Mott insulating [45], which appears to be the driving force behind the ordering instability.

GW + EDMFT results Previous model and *ab initio* GW + EDMFT calculations have shown that nonlocal correlation and screening effects are important for quantitatively accurate descriptions [46,47] and that they can drive the formation of electronic orders [48]. Also in the case of $La_3Ni_2O_7$, treating both the nonlocal and local physics in self-consistent GW + EDMFT has a significant effect on the electronic structure. It triggers a charge-order instability which breaks the symmetry between the two layers with period-2 oscillations for the original primitive cell, at first sight suggestive of a staggered ordering (two sublattices with interchanged occupations, see SM [28] for the pressure dependence). If we allow the spins to rearrange freely, this period-2 solution shows a ferromagnetic (FM) ordering. The difference to the predicted AFM order found in EDMFT can be understood from the filling and the generic phase diagram of the two-orbital Hubbard model [49], where AFM (FM) appears near 1/2 (3/4) filling. However, the calculation for a

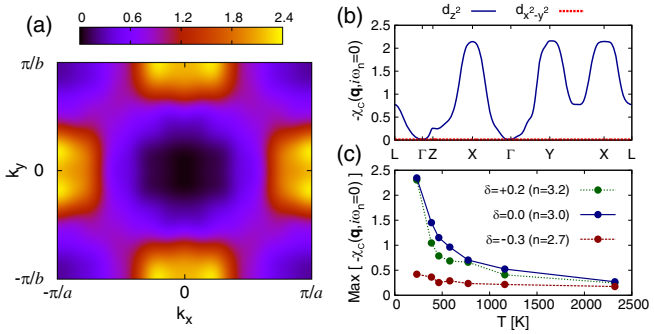

FIG. 4. Charge susceptibility $-\chi_c(\mathbf{q}, i\omega_n = 0)$ from $GW+$ EDMFT with suppressed charge order at $\beta = 50$ eV^{-1} (a) in the $\mathbf{k}_z = 0$ plane for $d_{x^2-y^2}$ and (b) along the indicated high-symmetry path. (c) Temperature and doping dependence of the maximum of $-\chi_c(\mathbf{q}, i\omega_n = 0)$.

supercell with two Ni dimers along the Ni—O—Ni bonds (see SM [28]) again produces period-2 oscillations, which shows that the order is not of the staggered type, and that the oscillations rather indicate an instability to a more complex ordering pattern.

To gain further insights into the ordering instability, and to get a better (beyond GW) description of the intrabilayer correlations, we perform calculations for a two-site impurity cluster in a rotated bonding-antibonding basis (see SM [28]). By neglecting the off-diagonal hybridizations in this basis, we can suppress the charge-ordering tendencies, and measure the charge susceptibility $\chi_c(\mathbf{q}, i\omega_n) = [1 - U_{\mathbf{q}}^{\mathrm{cRPA}}(i\omega_n)\Pi_{\mathbf{q}}(i\omega_n)]^{-1}\Pi_{\mathbf{q}}(i\omega_n)$ in the symmetrized state. Here, $\Pi_{\mathbf{q}}$ is the polarization from $GW+$ EDMFT, and $\omega_n = 2n\pi/\beta$ denotes bosonic Matsubara frequencies. In Fig. 4(b), we show $\chi_c(\mathbf{q}, i\omega_n = 0)$ along the indicated high-symmetry path to demonstrate that a charge instability can be expected to occur in the xy plane for the d_{z^2}-like orbital, while the $d_{x^2-y^2}$ orbital shows no ordering tendency. Focusing on the $k_z = 0$ plane in Fig. 4(a), we find a multipeak structure, with peaks centered around $(\pm(\pi/a), \pm\delta)$ and $(\pm\delta, \pm(\pi/b))$, with small δ, indicating the formation of diagonal stripes. The susceptibility for this type of order grows as temperature is lowered [Fig. 4(c)]. Along the stripes, we have a slow charge modulation with period $2\pi/\delta$ (in units of lattice spacing). Such an incommensurate charge density wave cannot be stabilized in simulations with a small unit cell. In particular, the ordering pattern is inconsistent with a simple staggering or with the doubled unit cell calculation that we have explicitly considered.

The reported results are robust against pressure changes in the $Fmmm$ phase, in the 20 GPa pressure range studied. While charge ordering has so far not been addressed directly for the high-pressure phase (specific heat measurements provide indirect evidence for its disappearance) [8,9,50,51], it is interesting to note that charge and spin order has been experimentally detected in the low-pressure phase of $La_3Ni_2O_7$ [9,50–52]. Reference [52] discussed possible ordering tendencies and their dependence on the oxygen deficiency of the experimental structure. They also proposed diagonal stripes of the incommensurate type, and in particular they mentioned the possibility of a sine-wave modulated charge ordering (charge density wave). Furthermore, an early theoretical study of the low-pressure phase emphasized that the 1D character of parts of the DFT Fermi surface suggests an instability to (striped) charge order [53]. An experimental confirmation of the presence or absence of charge stripes in the high-pressure phase would provide a check for the reliability of the $GW+$ EDMFT predictions.

TABLE II. Doping dependence of the orbital occupations per spin from $GW+$EDMFT for the nonordered and period-2 oscillating solution (filled site) at $\beta = 50$ eV^{-1}. Negative (positive) values correspond to hole (electron) doping.

	Suppressed order		Period-2 solution	
Doping	$n_{x^2-y^2}$	n_{z^2}	$n_{x^2-y^2}$	n_{z^2}
0.2	0.08	0.72	0.96	0.57
0.1	0.08	0.70	0.96	0.52
0.0	0.08	0.67	0.96	0.47
−0.1	0.08	0.64	0.95	0.43
−0.2	0.09	0.61	0.90	0.43
−0.3	0.09	0.59	0.85	0.43

The local spectral functions from the $GW+$EDMFT calculations are shown in Fig. 3(c). Only the d_{z^2} orbital has significant spectral weight close to the Fermi energy, both for the nonordered and period-2 solutions. In the latter case the nearly half-filled d_{z^2} orbital is found to be metallic, but close to a Mott transition, with a sharp quasiparticle peak split off from the doped upper Hubbard band, while in the 2/3-filled solution with suppressed order we find the familiar three-peak structure of a moderately correlated metal [see also the self-energies in panel (d)]. The dominance of the d_{z^2} orbital distinguishes $La_3Ni_2O_7$ from the infinite-layered nickelates or the cuprates, where the single-band description involves the $d_{x^2-y^2}$ orbital. This should have profound implications for the pairing symmetry.

We finally return to the previously mentioned self-doping effect due to the La layers, which has been eliminated by the structural relaxation. It is interesting to ask where holes introduced by the presence of such a pocket would end up. Self-consistent $GW+$EDMFT results for different doping levels (simulated by a shift of the chemical potential) are reported in Table II. In the electron doped and hole doped regime, the doped charge carriers initially go into the d_{z^2} orbital, while the almost empty or filled $d_{x^2-y^2}$ orbitals are little affected, especially in the case of suppressed charge order. Interestingly, upon hole doping, the susceptibility is markedly reduced compared to the nominal situation with

$n = 3$ electrons [Fig. 4(c)]. Hence, if self-doping occurs in the real material under pressure, this would suppress the charge order and potentially favor the superconducting state.

Conclusions.—Our self-consistent $GW + \mathrm{EDMFT}$ results for $La_3Ni_2O_7$ under pressure produce a markedly different physical picture than that obtained from DFT and DMFT. In particular, the self-consistent treatment of local and nonlocal screening and correlation effects results in an electronic structure with the d_{z^2} orbital as the main active player. While the period-2 oscillating solutions appear to be an artifact of a too small unit cell, the charge susceptibility reveals that $GW + \mathrm{EDMFT}$ predicts a charge instability toward the formation of diagonal stripes in the x-y plane, with the charge modulation in the d_{z^2} orbitals. In the broader context of high-temperature superconductivity, especially in cuprates, the role of fluctuating or static charge order has been much debated [54]. If such a competing or coexisting order exists also in the present bilayer nickelate superconductor is a relevant question that merits further experimental investigations. On the theory side, expanding the low-energy description to include La and O states will provide insights into the effects of the charge transfer from the O bands [12] and the role of the self-doping Γ pocket, which is found in the DFT calculations of the experimentally reported structure. This appears to be relevant since our calculations indicate a reduced charge ordering tendency upon hole doping.

We acknowledge support from the Swiss National Science Foundation via NCCR Marvel and Grant No. 200021-196966.

[1] V. I. Anisimov, D. Bukhvalov, and T. M. Rice, Phys. Rev. B **59**, 7901 (1999).
[2] D. Li, K. Lee, B. Y. Wang, M. Osada, S. Crossley, H. R. Lee, Y. Cui, Y. Hikita, and H. Y. Hwang, Nature (London) **572**, 624 (2019).
[3] S. Zeng, C. S. Tang, X. Yin, C. Li, M. Li, Z. Huang, J. Hu, W. Liu, G. J. Omar, H. Jani, Z. S. Lim, K. Han, D. Wan, P. Yang, S. J. Pennycook, A. T. S. Wee, and A. Ariando, Phys. Rev. Lett. **125**, 147003 (2020).
[4] M. Osada, B. Y. Wang, B. H. Goodge, K. Lee, H. Yoon, K. Sakuma, D. Li, M. Miura, L. F. Kourkoutis, and H. Y. Hwang, Nano Lett. **20**, 5735 (2020).
[5] G. A. t. Pan, Nat. Mater. **21**, 160 (2022).
[6] P. Worm, L. Si, M. Kitatani, R. Arita, J. M. Tomczak, and K. Held, Phys. Rev. Mater. **6**, L091801 (2022).
[7] N. N. Wang, M. W. Yang, Z. Yang, K. Y. Chen, H. Zhang, Q. H. Zhang, Z. H. Zhu, Y. Uwatoko, L. Gu, X. L. Dong, J. P. Sun, K. J. Jin, and J. G. Cheng, Nat. Commun. **13**, 4367 (2022).
[8] H. Sun, M. Huo, X. Hu, J. Li, Z. Liu, Y. Han, L. Tang, Z. Mao, P. Yang, B. Wang, J. Cheng, D.-X. Yao, G.-M. Zhang, and M. Wang, Nature (London) **621**, 493 (2023).
[9] Y. Zhang, D. Su, Y. Huang, H. Sun, M. Huo, Z. Shan, K. Ye, Z. Yang, R. Li, M. Smidman, M. Wang, L. Jiao, and H. Yuan, arXiv:2307.14819.
[10] Z. Luo, X. Hu, M. Wang, W. Wu, and D.-X. Yao, Phys. Rev. Lett. **131**, 126001 (2023).
[11] Y. Zhang, L.-F. Lin, A. Moreo, and E. Dagotto, arXiv:2306.03231.
[12] F. Lechermann, J. Gondolf, S. Bötzel, and I. M. Eremin, arXiv:2306.05121.
[13] E. Dagotto, Rev. Mod. Phys. **66**, 763 (1994).
[14] A. I. Lichtenstein and M. I. Katsnelson, Phys. Rev. B **62**, R9283 (2000).
[15] K.-W. Lee and W. E. Pickett, Phys. Rev. B **70**, 165109 (2004).
[16] P. Werner and S. Hoshino, Phys. Rev. B **101**, 041104(R) (2020).
[17] F. Lechermann, Phys. Rev. B **101**, 081110(R) (2020).
[18] K. Held, L. Si, P. Worm, O. Janson, R. Arita, Z. Zhong, J. M. Tomczak, and M. Kitatani, Front. Phys. **9**, 803 (2022).
[19] F. Aryasetiawan, M. Imada, A. Georges, G. Kotliar, S. Biermann, and A. I. Lichtenstein, Phys. Rev. B **70**, 195104 (2004).
[20] L. Hedin, Phys. Rev. **139**, A796 (1965).
[21] A. Georges, G. Kotliar, W. Krauth, and M. J. Rozenberg, Rev. Mod. Phys. **68**, 13 (1996).
[22] P. Sun and G. Kotliar, Phys. Rev. B **66**, 085120 (2002).
[23] S. Biermann, F. Aryasetiawan, and A. Georges, Phys. Rev. Lett. **90**, 086402 (2003).
[24] L. Boehnke, F. Nilsson, F. Aryasetiawan, and P. Werner, Phys. Rev. B **94**, 201106(R) (2016).
[25] F. Nilsson, L. Boehnke, P. Werner, and F. Aryasetiawan, Phys. Rev. Mater. **1**, 043803 (2017).
[26] P. Hohenberg and W. Kohn, Phys. Rev. **136**, B864 (1964).
[27] W. Kohn and L. J. Sham, Phys. Rev. **140**, A1133 (1965).
[28] See Supplemental Material at http://link.aps.org/supplemental/10.1103/PhysRevLett.131.206501, which includes Refs. [8,19,20,24,25,29–38], for the computational details and pressure dependence.
[29] K. Momma and F. Izumi, J. Appl. Crystallogr. **44**, 1272 (2011).
[30] J. P. Perdew, K. Burke, and M. Ernzerhof, Phys. Rev. Lett. **77**, 3865 (1996).
[31] The FLEUR group, The FLEUR project, http://www.flapw.de.
[32] N. Marzari and D. Vanderbilt, Phys. Rev. B **56**, 12847 (1997).
[33] A. A. Mostofi, J. R. Yates, Y.-S. Lee, I. Souza, D. Vanderbilt, and N. Marzari, Comput. Phys. Commun. **178**, 685 (2008).
[34] C. Friedrich, S. Blügel, and A. Schindlmayr, Phys. Rev. B **81**, 125102 (2010).
[35] P. Werner, A. Comanac, L. de' Medici, M. Troyer, and A. J. Millis, Phys. Rev. Lett. **97**, 076405 (2006).
[36] H. Hafermann, P. Werner, and E. Gull, Comput. Phys. Commun. **184**, 1280 (2013).
[37] P. Werner and A. J. Millis, Phys. Rev. Lett. **104**, 146401 (2010).
[38] M. Casula, P. Werner, L. Vaugier, F. Aryasetiawan, T. Miyake, A. J. Millis, and S. Biermann, Phys. Rev. Lett. **109**, 126408 (2012).

[39] F. Petocchi, V. Christiansson, F. Nilsson, F. Aryasetiawan, and P. Werner, Phys. Rev. X **10**, 041047 (2020).
[40] V. Christiansson, F. Petocchi, and P. Werner, Phys. Rev. B **107**, 045144 (2023).
[41] V. I. Anisimov, I. V. Solovyev, M. A. Korotin, M. T. Czyżyk, and G. A. Sawatzky, Phys. Rev. B **48**, 16929 (1993).
[42] M. T. Czyżyk and G. A. Sawatzky, Phys. Rev. B **49**, 14211 (1994).
[43] P. Werner and M. Casula, J. Phys. Condens. Matter **28**, 383001 (2016).
[44] C.-K. Chan, P. Werner, and A. J. Millis, Phys. Rev. B **80**, 235114 (2009).
[45] Without particle-hole symmetry, even in the Mott state, $-\mathrm{Im}\Sigma(i\omega_n)$ does not diverge as $\omega_n \to 0$.
[46] F. Petocchi, V. Christiansson, and P. Werner, Phys. Rev. B **104**, 195146 (2021).
[47] F. Petocchi, F. Nilsson, F. Aryasetiawan, and P. Werner, Phys. Rev. Res. **2**, 013191 (2020).
[48] S. Ryee, P. Semon, M. J. Han, and S. Choi, njp Quantum Mater. **5**, 19 (2020).
[49] S. Hoshino and P. Werner, Phys. Rev. B **93**, 155161 (2016).
[50] G. Wu, J. J. Neumeier, and M. F. Hundley, Phys. Rev. B **63**, 245120 (2001).
[51] Z. Liu *et al.*, Sci. China Phys. Mech. Astron. **66**, 217411 (2023).
[52] S. Taniguchi, T. Nishikawa, Y. Yasui, Y. Kobayashi, J. Takeda, S. Shamoto, and M. Sato, J. Phys. Soc. Jpn. **64**, 1644 (1995).
[53] D.-K. Seo, W. Liang, M.-H. Whangbo, Z. Zhang, and G. M., Inorg. Chem. **35**, 6396 (1996).
[54] B. Keimer, S. A. Kivelson, M. R. Norman, S. Uchida, and J. Zaanen, Nature (London) **518**, 179 (2015).